Journal of Natural Gas Science and Engineering xxx (2016) 1–8

Contents lists available at ScienceDirect

Journal of Natural Gas Science and Engineering

journal homepage: www.elsevier.com/locate/jngse

Evolution of shale apparent permeability from stress-controlled to displacement-controlled conditions

Mingyao Wei [a, b, *], Jishan Liu [a], Xiating Feng [a], Chunguang Wang [a, b], Fubao Zhou [c]

[a] State Key Laboratory of Geomechanics and Geotechnical Engineering, Institute of Rock and Soil Mechanics, Chinese Academy of Sciences, Wuhan 430071, China

[b] State Key Laboratory of Mining Disaster Prevention and Control Co-founded by Shandong Province and the Ministry of Science and Technology, Shandong University of Science and Technology, Qingdao 266590, China

[c] State Key Laboratory of Coal Resources and Safe Mining, China University of Mining and Technology, Xuzhou 221116, China

ARTICLE INFO

Article history:
Received 18 April 2016
Received in revised form
22 June 2016
Accepted 5 July 2016
Available online xxx

Keywords:
Apparent permeability
Boundary conditions
Adsorbed layer thickness
Permeability evolution

ABSTRACT

The apparent gas permeability of shale is determined by both the intrinsic permeability and the gas flow regimes. Although a considerable amount of studies has been conducted to understand how flow regimes affect the apparent permeability, the impact of the intrinsic permeability has not been understood well. In this study, we introduced an intrinsic permeability model under variable stress conditions and the impact of the adsorbed layer thickness into a typical apparent permeability model. Our model was verified through comparisons of our model results with the experimental data in the literature. The new apparent permeability model was applied to evaluate the evolution of shale permeability under a spectrum of boundary conditions from stress-controlled to displacement-controlled conditions. Our model results demonstrate that the evolution of gas permeability is controlled by the change in intrinsic permeability under high pressures and by the flow regimes under low pressures. Because the change in intrinsic permeability is dependent on the boundary conditions, the evolution of apparent gas permeability is also boundary-dependent. When the shale is stress-controlled, the gas permeability increases with pressure under the constant confining stress condition. When the shale is under displacement-controlled, the gas permeability decreases with pressure under the constant volume condition.

1. Introduction

Shale gas is known as unconventional gas reservoirs with low permeability and a high contrast of transport properties between matrix and fracture. Experimental studies of shale indicate that the pore size is wide distributed and predominantly between 1.6 and 69.0 nm (Clarkson et al., 2012a,b; Liu et al., 2015). In addition, the estimated pore radius distributions show that smaller pores dominate the distribution. Pores in shale are in the range of nanometer to micrometer scale that can be construed as nano- or micro-channels. In shale gas systems, these pores allow gas flow from shale to induced fractures along the flow-path network during production.

Even though these small pores may not contribute significantly to porosity, they have a significant effect on permeability and consequently on the flow of gas through tight porous media (Rahmanian et al., 2010). In general, the conventional Darcy equation cannot fully capture the physics of flow in the nanopore structure of shale reservoirs. This is because the increasing number of molecular collisions with the pore walls as a source of momentum transfer diminishes the validity of the standard continuum approach with no-slip boundary conditions, as the length scale of the physical system decreases. Gas slippage occurs when the pore size approaches the mean free path of the gas molecules causing the gas molecules to slip on the rock surface and to accelerate. The narrower the flow diameter and the larger mean free path of the gas molecules, the greater the anticipated slippage effect (Rahmanian et al., 2010). Great efforts have been devoted to understanding and modelling of micro-scale flow considerations in shale sediment by other researchers, both theoretically and experimentally (Javadpour et al., 2007; Florence et al., 2007; Civan, 2010; Sakhaee-Pour and Bryant, 2012). Among the methods proposed, apparent-permeability correlation is one of the most widely

* Corresponding author. State Key Laboratory of Geomechanics and Geotechnical Engineering, Institute of Rock and Soil Mechanics, Chinese Academy of Sciences, Wuhan 430071, China.
E-mail address: mywei@whrsm.ac.cn (M. Wei).

http://dx.doi.org/10.1016/j.jngse.2016.07.012
1875-5100/

accepted approaches, with which we can integrate the recent achievement of nanoscale flow modelling in a permeability-correlation term (Niu et al., 2013). Several methods were presented to determine the apparent-permeability correlation (Civan, 2010; Beskok and Karniadakis, 1999; Javadpour, 2009). In all of these studies, the intrinsic permeability was assumed constant.

On the other hand, experimental studies have demonstrated that the shale permeability could change by several orders of magnitude under different geomechanical conditions (Schloemer and Krooss, 1997; Neuzil, 1994). Several models have been proposed to explain the variability of intrinsic permeability induced by effective stress and matrix sorption deformation. The potential effect of sorption-induced swelling on the evolution of coal permeability have been investigated through experimental and analytical studies (Pan et al., 2010; Robertson and Christiansen 2005). Under constant total stress, gas permeability decreases with the increase in pore pressure due to coal swelling (Robertson and Christiansen 2005; Pan and Connell, 2011), and increases with the decrease in pore pressure due to matrix shrinkage (Cui and Bustin, 2005; Harpalani and Schraufnagel, 1990). These coal permeability models can be divided into two important classes: those under uniaxial strain conditions and those under triaxial stress conditions Liu et al. (2011a,b) developed a more general approach, which characterizes the evolution of intrinsic permeability under a full spectrum of mechanical conditions from stress-controlled to displacement controlled swelling/shrinkage conditions. However, these models did not include the effect of flow regimes.

Quantification of the apparent gas permeability can be accomplished by correction of the relevant prevailing flow regimes as characterized by their Knudsen number, which is the ratio of the mean free path of the gas under *in-situ* conditions to pore diameter. Normally, the pore radius is assumed invariant in most previous permeability models. However, the volume of the adsorbed layer is sufficiently large to affect the pore radius, because the radius is at nanoscale. Xiong et al. (2012) indicated that correction of permeability may, however, be insufficient in the presence of adsorption, where the decrease of pore diameter occupied by adsorbed gas molecules may be significant with high TOC and large hydrocarbon contents in place. In the presence of adsorption, there is a pore pressure dependent loss of porosity and cross-sectional area of pore channels. Cui and Bustin (2009) considered the influence of the adsorbed layer on the void space and the adsorbed porosity. In addition, the volume of adsorbed gas was estimated using reservoir simulation (Cipolla et al., 2010). Jin et al. (2015) measured the shale permeability with three different gases (argon, nitrogen, and carbon dioxide) as the permeating fluid. Generally, samples have higher measured permeabilities when using nitrogen as the pore fluid rather than using argon, even at high pressure to render slippage effects negligible. Argon has a similar sorption potential to methane while that nitrogen is relatively weak. Sakhaee-Pour and Bryant (2012) analyzed the effects of adsorbed layers on the apparent permeability under different reservoir conditions for a simple pore network based on experimental data and showed that permeability is overestimated at high pressures. Ambrose et al. (2010) indicated that the volume of the adsorbed layer, which occupies the pore volume available for free gas storage, is a function of gas species, temperature and pressure. Xiong et al. (2012) modified the transport equation to account for volume lost due to the volume occupied by the adsorbed gas based on an assumption of monolayer adsorption. Although many previous studies have contributed to improvements in understanding of the effect of adsorbed layers on apparent permeability, permeability models considering this effect have not been well developed.

In this study, we introduced an intrinsic permeability model under variable stress conditions and the effect of the adsorbed layer thickness into the typical apparent permeability model. The new apparent permeability model was applied to evaluate the evolution of shale permeability under a spectrum of boundary conditions ranging from stress-controlled to displacement-controlled conditions.

2. Nanopore space evolution with gas adsorption

In this section, we first discuss introduce a gas adsorption model based on pore volume filling/potential theory and then establish an equation to quantify the decrease in pore radius induced by the adsorption layer.

2.1. Gas adsorption model

The monolayer Langmuir isotherm is generally applied to describe the gas adsorption behavior in shale gas reservoirs. However, it has been noted recently that the Langmuir isotherm may give poor results when used to estimate the amount of gas adsorbed in shale that is rich in organic carbon (Clarkson et al., 1997). This assumption of monolayer adsorption leads to neglect of the effect of adsorbed layer thickness. Actually, natural gas adsorbed on organic carbon surfaces forms a multi-molecular layer at high reservoir pressures. Previous molecular dynamics calculations showed that the Langmuir isotherm could not adequately describe methane adsorption to the nanopores in the organic material of the shale (Sigal et al., 2013; Yu et al., 2014). Some researchers have suggested that equations based on pore volume filling/potential theory may provide better results than the Langmuir equation for both high-pressure (up to 10 MPa) and low-pressure (<0.127 MPa) (Clarkson et al., 1997). Sakurovs et al. (2007) suggested that gas sorption mechanism was more like a pore-filling type than monolayer coverage. Accordingly, using the Dubinin-Radushkevich (D-R) equation (Sakurovs et al., 2008, 2010) to model the shale adsorption isotherm then yields:

$$W_{ads} = W_0 \exp\left(- D\left[ln\left(\frac{\rho_a}{\rho_G}\right)\right]^2\right) \quad (1)$$

where W_{ads} is absolute adsorption of the shale gas, W_0 is the maximum sorption capacity of the shale, ρ_G is the density of the gas at the temperature and pressure, ρ_a is the gas density of adsorbed phase (generally assumed to be the van der Waals density of the gas (Sakurovs et al., 2010) and is 370 kg/m^3 for CH_4 typically through MD simulation (Ambrose et al., 2010), and D is a constant (Sakurovs et al., 2009). The term D can be further expressed as: $D = (RT/\beta E)^2$, where R is the ideal gas constant, T is the absolute thermodynamic temperature, E is the heat of adsorption and β is the affinity coefficient of the gas to the substrate (White et al., 2005). The D-R equation is established according to the fact that the surface to be covered by potential adsorption sites on average has a constant areal density.

2.2. Model of adsorption-induced change in pore radius

Microstructural investigation of nanopore geometries based on backscattered electron (BSE) images indicates that nanopores are typically round in cross-section (Curtis et al., 2012). Thus, it is reasonable to consider all nanopores in cross-section as spheres with an average pore radius r, as shown in Fig. 1. Since the exposed surface area is larger in nanopores than in micropores, these nanopores are an ideal place for trapping gas (molecule size 0.38 nm) in the adsorbed state. The thickness of the adsorbed layer becomes comparable to the nano pore radius because the adsorbed

Please cite this article in press as: Wei, M., et al., Evolution of shale apparent permeability from stress-controlled to displacement-controlled conditions, Journal of Natural Gas Science and Engineering (2016), http://dx.doi.org/10.1016/j.jngse.2016.07.012

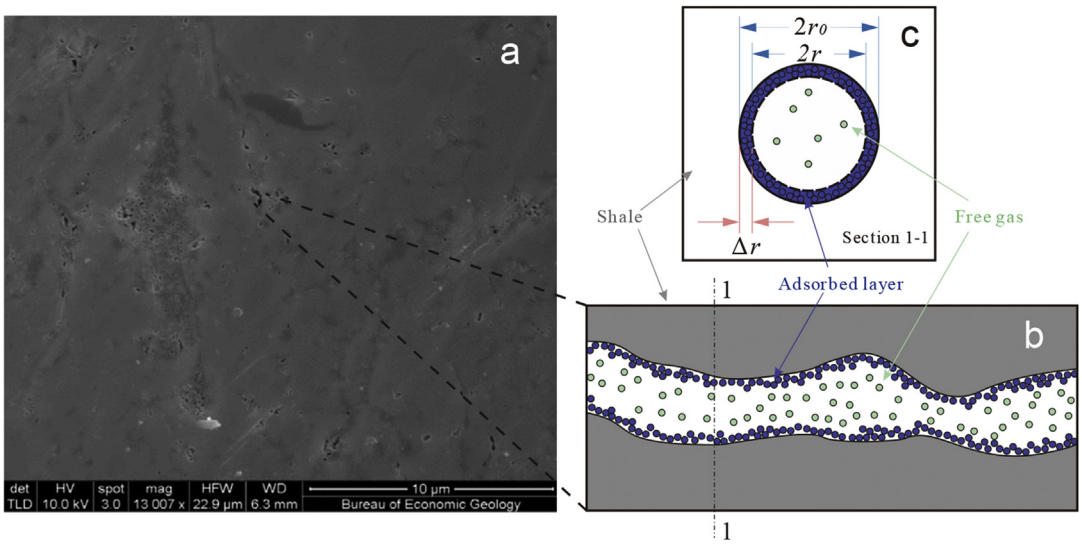

Fig. 1. (a) A SEM image of shale surface revealing existence of pores in kerogenic materials from Etminan et al. (2014). (b) A zoomed-in schematic diagram of the pore inside kerogenic material. Free state gas molecules (green dots) can flow through pore space. Adsorbed gas (blue dots) exists as compressed gas layer on the pore surface. (c) A diagram of idealized nano pore with an initial radius of $2r_0$. The radius is reduced to $2r$ by adsorbed layer after gas adsorption. (For interpretation of the references to colour in this figure legend, the reader is referred to the web version of this article.)

gas is present in abundance (Sigal et al., 2013). By accounting for the volume consumed by the adsorbed gas on the pore surface, the space available for the free gas is naturally reduced.

It is evident that the thickness of adsorbed layer affects the nanopore radius. The nanopore radius can be obtained as:

$$r = r_0 - \Delta r \tag{2}$$

where r is the average nanopore radius, r_0 is the initial nanopore radius, Δr is the thickness of adsorbed layer.

Assuming that shale gas is adsorbed evenly on the pore surface, the average thickness of the adsorbed layer then depends on the sorption capacity W_{ads} and the specific surface area S. The specific surface area of the shale sample is a parameter that can be easily obtained from the adsorption isotherms. The average thickness of the adsorbed layer can be expressed as:

$$\Delta r = \frac{W_{ads}}{\rho_a S} = \frac{W_0}{S\rho_a}\exp\left(-D\left[ln\left(\frac{\rho_a}{\rho_G}\right)\right]^2\right) = t_a\exp\left(-D\left[ln\left(\frac{\rho_a}{\rho_G}\right)\right]^2\right) \tag{3}$$

where S is specific surface area, and t_a is the thickness of the adsorbed layer at extremely high pressure.

Substituting Eq. (3) into Eq. (2) yields:

$$r = r_0 - t_a\exp\left(-D\left[ln\left(\frac{\rho_a}{\rho_G}\right)\right]^2\right) \tag{4}$$

Eq. (4) expresses the relationship between pore radius and gas density, that indicates the nanopore radius decreases exponentially along with growing thickness of the adsorbed layer.

3. An apparent permeability model for the shale matrix

Unconventional shale gas sediments are characterized by their rich abundance of nanopores. Consequently, the microstructural features of the shale affect the capacities of the sediments in generating, storing, and producing gas. A widely recognised dimensionless parameter that determines the degree of appropriateness of the continuum model is the Knudsen number (Kn). For Knudsen numbers less than 0.01, the use of the ideal gas constant in Darcy's law and the assumption of continuum flow remain valid. For Knudsen numbers greater than 0.01, an effective permeability must be computed to compensate for Knudsen diffusion and/or slippage flow. Beskok and Karniadakis (1999) developed a unified model for gas flow in micro-tubes that is valid over the entire range of flow regimes. Florence et al. (2007) derived the following model, which relates the apparent permeability k_a to the intrinsic permeability k_∞:

$$k_a = k_\infty(1+\beta k_n)\left(1+\frac{4K_n}{1+K_n}\right) \tag{5}$$

As discussed above, the gas flow state in nanopores is determined by not only the gas pressure but also by the nanopore radius. The Knudsen number is defined as the ratio of the gas mean-free-path λ and the pore diameter 2r. According to Eq. (4), the Knudsen number is defined as:

$$K_n = \frac{\lambda}{2r} = \frac{\lambda}{2\left(r_0 - t_a\exp\left(-D\left[ln\left(\frac{\rho_a}{\rho_G}\right)\right]^2\right)\right)} \tag{6}$$

where the mean free path of the gas λ is defined as:

$$\lambda = \frac{B_k T}{\sqrt{2}\pi d_g^2 P} \tag{7}$$

in which B_k is the Boltzmann constant; d_g is the effective molecular diameter and P is the gas pressure. The parameter β is a dimensionless rarefaction coefficient. The variation of the β-parameter as a function of Kn is represented thus (Beskok and Karniadakis, 1999):

$$\beta = \frac{128}{15\pi^2}\tan^{-1}\left(4K_n^{0.4}\right) \tag{8}$$

When gas produced in shale reservoirs, the drop in gas pressure then alters the correlation coefficient of the gas flow state, through

Please cite this article in press as: Wei, M., et al., Evolution of shale apparent permeability from stress-controlled to displacement-controlled conditions, Journal of Natural Gas Science and Engineering (2016), http://dx.doi.org/10.1016/j.jngse.2016.07.012

both desorption-induced radius increase and pressure-induced mean free path increase, as defined in Eqs. (6) and (7) respectively. Eq. (5) is able to capture continuum, transition, and Knudsen flow in shale matrix. Note that the Knudsen flow relies only on the Knudsen number and the intrinsic permeability of the porous medium. It means that the permeability evolution affected by effective stress is not included in the apparent permeability model.

4. Evolution of permeability from stress-controlled to displacement-controlled conditions

4.1. A multi-scale model for the shale matrix

The change in effective stress varies the porosity and permeability of the shale sediments. Therefore, the intrinsic permeability does not remain constant during shale gas extraction. To investigate the effective stress effect, we consider intrinsic permeability as the absolute permeability instead. According to our previous work on the effective strain-based absolute permeability model (Liu et al., 2011a,b), the intrinsic permeability can be described as:

$$\frac{k_\infty}{k_0} = \left(1 + \frac{\alpha}{\varphi_0}\Delta\varepsilon_e\right)^3 \tag{9}$$

where the effective strain increment is calculated by:

$$\Delta\varepsilon_e = \Delta\varepsilon_v - \frac{\Delta P}{K_s} + \Delta\varepsilon_s \tag{10}$$

where φ_0 and k_0 are the initial porosity and permeability of the matrix, $\Delta\varepsilon_e$ is defined as the total effective volumetric strain increment, $\Delta\varepsilon_v$ is total volumetric strain increment, $\Delta P/K_s$ is the change in compressive strain, α is the Biot coefficient, $\Delta\varepsilon_s$ is the gas sorption-induced volumetric strain increment and K_s represents the bulk modulus of the shale grains. Eq. (9) is the shale permeability model derived from the fundamental principles of poroelasticity, and it is applicable to the evolution of permeability under different boundary conditions at a macroscopic scale. However, this model did not include the effect of flow regimes.

In order to combine the apparent permeability model and effective stress based permeability model, the following basic assumptions are made:

(1) The effect of effective stress on the change in nanopore diameter is negligible.
(2) Shale is a homogeneous, isotropic, dual poroelastic continuum without fractures, and the system is isothermal.
(3) Shale is an idealized porous medium composed of identical, homogeneous distributed, nanopores.

Substituting Eq. (9) into Eq. (5), the multi-scale permeability model for shale matrix is defined as:

$$k_a = k_0\left(1 + \frac{\alpha}{\varphi_0}\Delta\varepsilon_e\right)^3 (1 + \beta K_n)\left(1 + \frac{4K_n}{1 + K_n}\right) \tag{11}$$

This new model fully considers the both effect of effective stress under macroscopic scale and flow regimes at the microscopic scale. This new model of apparent permeability based on multi-physics at different scales can be applied to reservoir evaluation and production optimization. Note that both the apparent and permeability absolute permeability are discussed for single phase flow in this work. In the following sections, this new model is applied to a series of cases commonly used in laboratory tests and theoretical analyses to generate typical response curves.

4.2. Constant volume tests

In this section, the new multi-scale permeability model will be developed for constant volume condition and constant stress condition. In constant volume tests (or displacement-controlled tests), the boundary deformation is held at zero to maintain a constant total volume. When a shale sample is completely constrained, a force and its associated strain then develop within the shale matrix, which is induced by gas sorption (Liu et al., 2011a,b). In this case, Eq. (11) can be written as:

$$k_a = k_0\left(1 - \frac{\alpha}{\varphi_0}\varepsilon_s\right)^3 (1 + \beta K_n)\left(1 + \frac{4K_n}{1 + K_n}\right) \tag{12}$$

$$\varepsilon_s = \varepsilon_L \exp\left(-D\left[ln\left(\frac{\rho_a}{\rho_G}\right)\right]^2\right) \tag{13}$$

where ε_s is the gas sorption-induced strain, and is linearly proportional to the amount of gas adsorption, and ε_L is the matrix swelling/shrinkage constant that represents the maximum swelling capacity.

4.3. Stress-controlled tests

Stress-controlled tests are widely used for triaxial or hydrostatic tests. When the response is controlled completely by stress alone, no additional force or associated strain develops within the shale. Defining the initial permeability as the permeability subject to an initial confining stress under extremely low gas pressure, Eq. (11) can be simplified to:

$$k_a = k_0\left(1 + \frac{\alpha}{\varphi_0}\frac{\Delta P}{K}\right)^3 (1 + \beta K_n)\left(1 + \frac{4K_n}{1 + K_n}\right) \tag{14}$$

The effect of stress on permeability is ignored because the effective stress induced by the confining pressure under changing gas pressure is invariant. In addition, the effective stress directly induced by pore pressure determines the permeability evolution in stress-controlled tests. It also shows that the strain induced by matrix swelling/shrinkage has no influence on permeability.

5. Model validation

5.1. Model validation under constant stress conditions

This multi-scale permeability model is validated by using the experimental data from Sinha et al. (2013) and Letham (2011) as shown in Figs. 2 and 3, respectively. The ratios of apparent permeability to the permeability at infinite pressure were measured by Sinha et al. (2013) and Letham (2011) at different pressures using helium and methane, respectively. The Klinkenberg model used in previous studies adequately described the deviation from Darcy's law for permeability values in the case of helium, but failed to account accurately for the deviation when using methane, which is a sorbing gas. Our new permeability model, which comprising nanopore flow mechanics and adsorbed layer effects, is validated with the experimental data below. Note that experiments were conducted under constant stress conditions in which effective stress was directly affected by the pore pressure.

Sample 1 from Sinha et al. (2013) was found to have a TOC content of 8.52% by mass respectively. The positive correlation between the sorbed gas capacity and the TOC concentration is widely used as an indicator of gas quality. Comparison of the TOC content of this sample to other rocks with known Langmuir

Please cite this article in press as: Wei, M., et al., Evolution of shale apparent permeability from stress-controlled to displacement-controlled conditions, Journal of Natural Gas Science and Engineering (2016), http://dx.doi.org/10.1016/j.jngse.2016.07.012

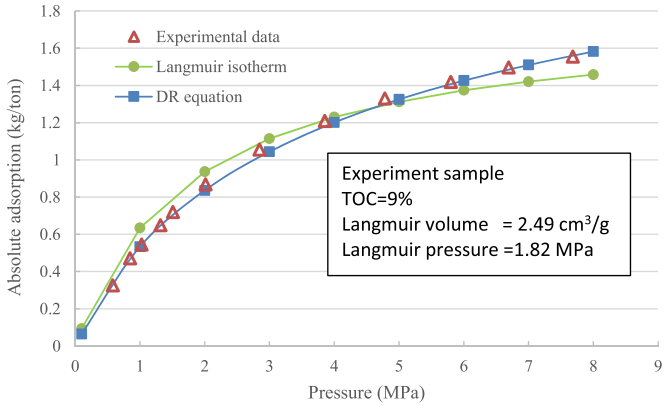

Fig. 2. Adsorption on samples from Letham (2011) with DR equation and Langmuir equation. The Langmuir parameters are estimated by comparison with samples from same reservoir.

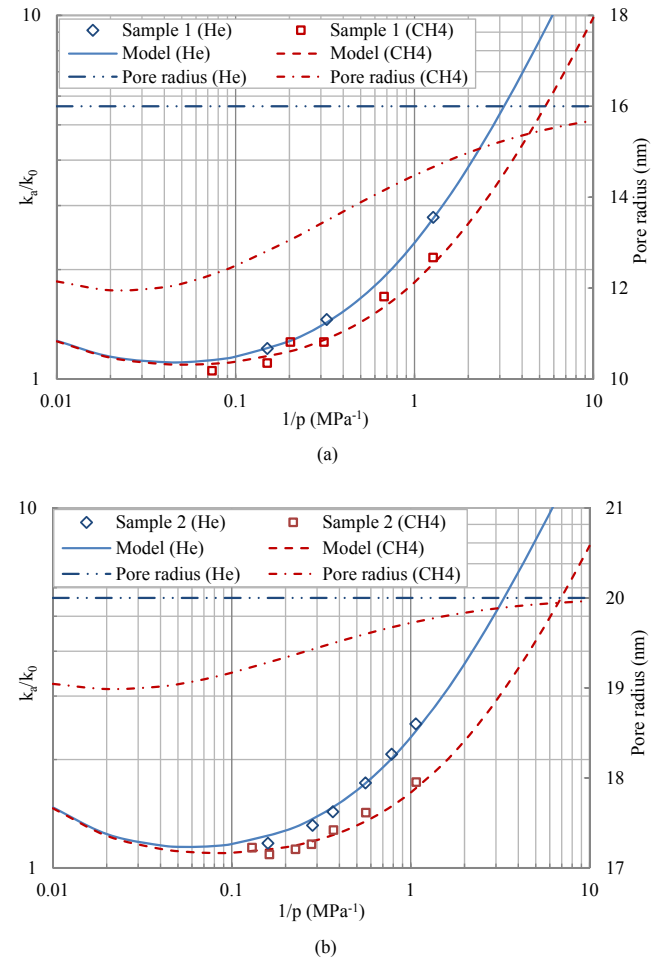

Fig. 3. Fitting results of the permeability model to experimental data under constant stress condition. Experimental data in (a) is from Sinha et al. (2013), and in (b) from Letham (2011).

parameters led to an estimated Langmuir pressure of 1.82 MPa and a Langmuir volume of 2.49 cm^3/g. The fitting curves to the experimental data using the D-R equation and the Langmuir equation are plotted in Fig. 2, and the parameters used for Sample 1 in the fitting are listed in Table 1. The Langmuir parameters are estimated by comparison with samples from same reservoir due to the lack of experimental data from the original reference. It shows that the D-R equation gives a better fits to the data than the Langmuir equation, which indicated that the D-R equation was more suitable for use when describing the adsorption in shale materials.

Fig. 3 shows satisfactory agreement between results calculated from Eq. (14) and the experimental data. It can be seen that the differing permeability to helium and methane was due to the change in pore radius. Specifically, the pore radius remained constant during helium desorption but increased during methane desorption, hence leading to the deviating permeability curves of helium and methane when the gas pressure decreased. Thus, permeability measurements at the lower pressures that are typical in the later stages of shale gas production must be conducted to detect the differences in permeability due to desorption. Otherwise, an overestimated of the permeability would occur because the influence of adsorbed gas layer was neglected.

At the stage of high gas pressure, the apparent permeability increased with increasing gas pressure, because the effective stress decreased with gas pressure, as shown by Eq. (14). Fig. 3 shows that the new model adequately represents experimental observations by considering the effect of the adsorbed layer on permeability.

5.2. Model validation under uniaxial stress conditions

In order to validate the new model under uniaxial stress conditions, a triaxial holder was utilized for measuring coal permeability. The axial direction of the cylindrical sample was constrained by a fixed displacement boundary, and the circumferential boundary was purely stresscontrolled by use of a pump. The initial stress on each coal sample was set to 9 MPa and 12 MPa before the experiment began, respectively. The helium was used for measurements as a test gas instead of an adsorptive ga (sorption-induced strain thus be ignored). Note that coal samples were continuous, intact, and without visible fractures.

The comparison between filed data and the simulation results is shown in Fig. 4. It was noticeable that the simulation results were all in good agreements with the experimental data. Shale permeability increased with decreasing gas pressure due to the effects of the prevailing flow regimes. However, this effect on shale permeability diminishes at high gas pressure. The evolution of shale permeability was dominated by effective stress as the gas pressure increased. By combining the effect of slippage flow and effective stress, matrix permeability revealed complex behavior.

6. Permeability evolution under different boundary conditions

In this section, we use our newly developed model to derive permeability evolution for shale under different boundary conditions ranging from stress-controlled to displacement-controlled states.

6.1. Permeability evolution under constant stress condition

The apparent permeability, intrinsic permeability and initial permeability reveal shale characteristics from different perspectives. The apparent permeability is defined in Eq. (11), which compounds the intrinsic permeability with the complexity of flow in nanopores. Intrinsic permeability is related to the macroscopic-scale properties determined by the effective stress, and the initial permeability considers the initial status. The relationship between these three values during gas production was plotted in Fig. 5. The ratio of apparent permeability to initial permeability

Please cite this article in press as: Wei, M., et al., Evolution of shale apparent permeability from stress-controlled to displacement-controlled conditions, Journal of Natural Gas Science and Engineering (2016), http://dx.doi.org/10.1016/j.jngse.2016.07.012

Table 1
Fitted parameters for shale samples.

Identity	Values		
	Sample 1 (Sinha et al., 2013)	Sample 2 (Letham, 2011)	Sample 3 (coal)
Max sorption capacity W_0	3.0 kg/ton	3.0 kg/ton	–
Parameter D	0.07	0.09	–
Specific surface area S	2 m^2/g	8 m^2/g	–
Gas density of adsorbed phase ρ_a	370 kg/m^3	370 kg/m^3	–
Initial nanopore radius r_0	16 nm	19.5 nm	40 nm
Bulk modulus K_s	25 GPa	15 GPa	4 GPa
Initial porosity	5%	5%	5%
Biot coefficient α	1	–	–
Volumetric strain coefficient ε_L	0.01	–	–

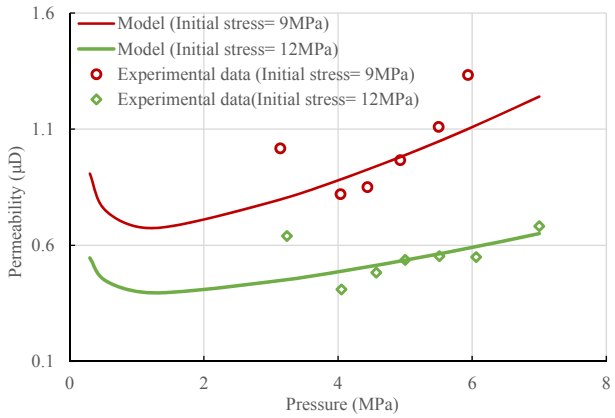

Fig. 4. Fitting results of the permeability model to experimental data under constant displacement condition.

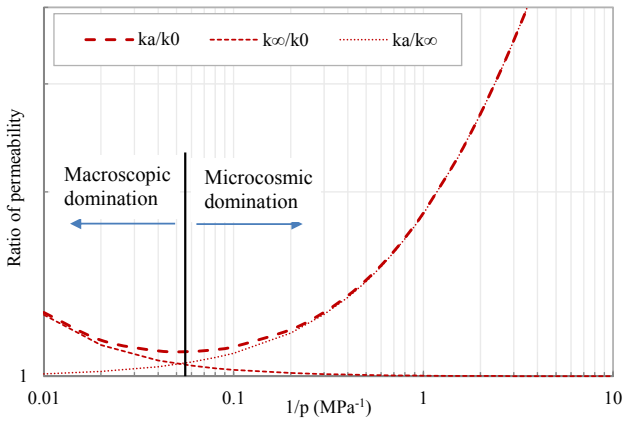

Fig. 5. Permeability evolution under constant stress condition.

exhibited a non-monotonic variation with gas pressure drawdown. For further analysis, the ratio of apparent permeability to intrinsic permeability and the ratio of intrinsic permeability to initial permeability are plotted using different line types. Upon gas pressure drawdown, the ratio of apparent permeability to intrinsic permeability increased due to the presence of stronger slippage flow, but the ratio of intrinsic permeability to initial permeability decreased since the effective stress increased due to decreasing pore pressure. These two curves exhibited opposite trends and thus, the apparent permeability was significantly affected by macroscopic-scale stress under high pressure, but primarily by the influence of slippage flow when the gas pressure was relatively low.

6.2. Permeability evolution under constant volume conditions

Similar to the constant stress case, the apparent permeability is under the combined influence of macroscopic-scale stress and slippage flow. In contrast to the constant stress condition, the macroscopic-scale stress has a reversed impact on the apparent permeability under constant volume conditions, as seen in Fig. 6. This is because the desorption-induced increase in pore volume resulted in a significant increase in cross-section in the flow pathways, in turn causing a significant increase in the permeability ratio. In particular, the apparent permeability increases significantly under high pressure. By combining the effect of macroscopic-scale stress and slippage flow, the apparent permeability increases continuously with gas pressure drawdown under constant volume conditions. It can therefore be inferred that the rate of production of shale gas is mainly related to macroscopic-scale geomechanics during the primary recovery stage, whereas shale productivity significantly depends on nano-scale flow at low pore pressure.

7. Influence of adsorbed layer at different initial nanopore radius

This section investigates the parameter sensitivities of the proposed apparent permeability model under constant stress conditions.

For conventional rock, the effect of adsorbed gas can be ignored in flow modelling flow because of the large total void space compared with the volume occupied by adsorption. However, the adsorbed volume of CH_4 is crucial in shale because the pore radius is often smaller than 5 nm and much of the void space existing in

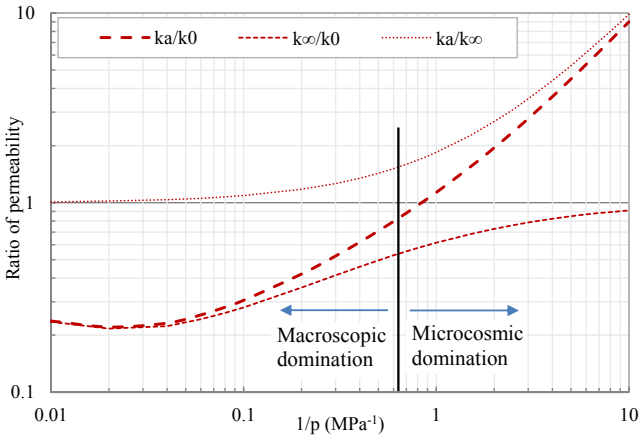

Fig. 6. Permeability evolution under constant volume condition.

Please cite this article in press as: Wei, M., et al., Evolution of shale apparent permeability from stress-controlled to displacement-controlled conditions, Journal of Natural Gas Science and Engineering (2016), http://dx.doi.org/10.1016/j.jngse.2016.07.012

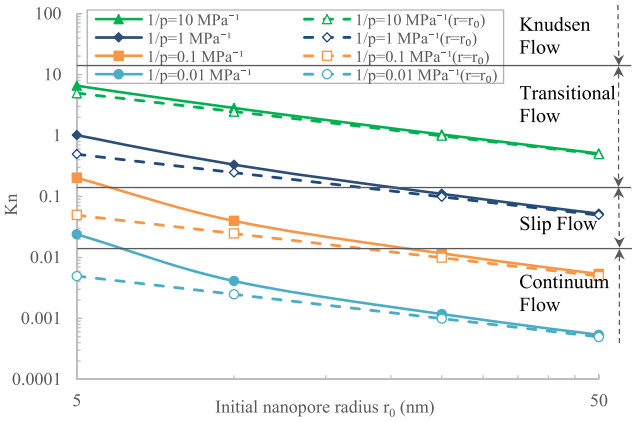

Fig. 7. Effect of adsorbed layer on *Kn* with different initial pore radius.

organic material, for which CH_4 has a large affinity (Sakhaee-Pour and Bryant, 2012). Nanopore radius plays an important role in shale gas production because a higher mass transfer of gas molecules occurs inside the nanopores.

The micro-scale flow of shale gas through porous media involves various distinct transport mechanisms according to the Knudsen number. Fig. 7 shows the range of flow regimes in shale gas reservoirs depending on the pore radius and the pressures of those reservoirs. The Knudsen number mainly lies between 0.001 and 10 for all pressure from 0.1 to 100 MPa when the pore radius is between 5 and 50 nm. For a pore radius assumed constant, the Knudsen number is smaller due to the decreasing volume occupied by the adsorbed layer. Moreover, the influence of the adsorbed layer on the Knudsen number is less pronounced for larger pores.

Fig. 8 shows the ratio of apparent permeability to initial permeability for different initial pore radius To evaluate the effect of the adsorbed layer on the apparent permeability, comparison curves where pore radius is assumed constant, (*i.e.*, where the adsorption thickness is ignored) have been added to the figure. The differences between the solid lines and the dash lines in the figure are noticeable when the pore radius is less than 25 nm, indicating that the adsorbed layer has greater influence on increasing slippage flow inside small radius nanopores thar are abundant in shale. It can also be seen that the influence of the adsorbed layer is more important in estimating the permeability at lower pressure. The permeability of a shale reservoir is predicted to increase

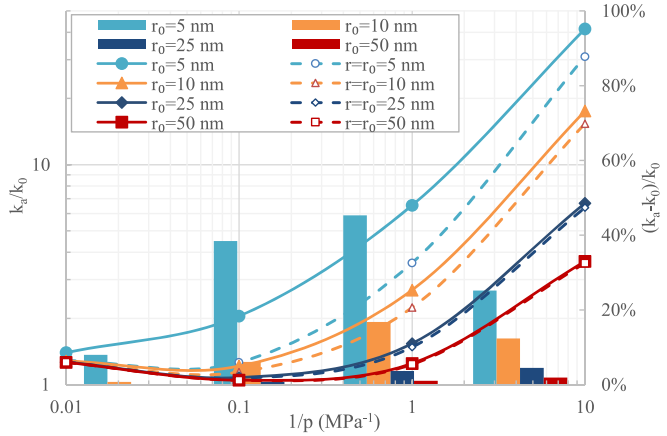

Fig. 8. Effect of adsorbed layer on apparent permeability for different pore radius under constant stress condition.

significantly over the life of a well, by a factor of ten or more, as the production continues and the pressure decreases.

8. Conclusions

A new apparent gas permeability model for shale was presented to provide significant improvement for studying gas transport in multi-scale. In this model, the apparent permeability varies as a function of the effective stress and Knudsen number, and the impact of the adsorbed layer thickness was also included. This multi-scale permeability model is also validated by experimental data under constant stress condition and uniaxial stress condition. Model results were all in good agreement with these experimental data. We applied the model to evaluate the evolution of apparent permeability under various boundary conditions ranging from stress-controlled to displacement-controlled cases. Based on the model results, the following conclusions can be drawn:

(1) The new apparent permeability model fully considers both the influences of effective stress at the macroscopic scale and flow regimes ar the microscopic scale. Our model also demonstrates that the apparent permeability is significantly affected by macroscopic-scale stress under high pressure, but is primarily influenced by flow regime when the gas pressure is relatively low. This suggested that shale gas production is mainly determined by the evolution of effective stress during the primary recovery stage. The impact of flow regimes may be important only at a late stage when the gas pressure is very low.

(2) Gas permeability is significantly greater with higher gas sorption capacity compared to that is without adsorption. The permeability would be underestimated where it not for the consideration of the influence of the gas adsorbed layer. It also suggested that the effect of the adsorption layer on the permeability ratio is more significant in the later stages of gas production, especially in shale that has a smaller average pore radius.

Acknowledgements

This work was funded partially by Natural Science Foundation of China (51504235) (51474204) (51408345), The State Key Laboratory of Coal Resources and Safe Mining, CUMT (13KF05) (SKLCRSM14KFA01), Opening Project Fund of State Key Laboratory of Mining Disaster Prevention and Control Co-founded by Shandong Province and the Ministry of Science and Technology (MDPC2013KF03), the Fundamental Research Funds for the Central Universities (Grant No. 2015XKZD03). These supports are gratefully acknowledged.

References

Ambrose, R.J., Hartman, R.C., Diaz-Campos, M., Akkutlu, I.Y., Sondergeld, C.H., 2010. New pore-scale considerations for shale gas in place calculations. In: SPE Unconventional Gas Conference. Pittsburgh, PA SPE-131772.

Beskok, A., Karniadakis, G.E., 1999. A model for flows in channels, pipes, and ducts at micro and nano scales. Microscale Thermophys. Eng. 3 (1), 43–77.

Civan, F., 2010. Effective correlation of apparent gas permeability in tight porous media. Transp. Porous Media 82 (2), 375–384.

Cipolla, C.L., Lolon, E.P., Erdle, J.C., et al., 2010. Reservoir modeling in shale-gas reservoirs. SPE Reserv.Eval. Eng. 13 (4), 638–653.

Clarkson, C.R., Bustin, R.M., Levy, J.H., 1997. Application of mono/multilayer and adsorption potential theories to coal methane isotherms at elevated temperature and pressure. Carbon 35 (12), 1689–1705.

Clarkson, C.R., Jensen, J.L., Chipperfield, S., 2012a. Unconventional gas reservoir evaluation: what do we have to consider? J. Nat. Gas Sci. Eng. 8, 9–33.

Clarkson, C.R., Jensen, J.L., Pedersen, P.K., et al., 2012b. Innovative methods for flow-unit and pore-structure analyses in a tight siltstone and shale gas reservoir. AAPG Bull. 96 (2), 355–374.

Please cite this article in press as: Wei, M., et al., Evolution of shale apparent permeability from stress-controlled to displacement-controlled conditions, Journal of Natural Gas Science and Engineering (2016), http://dx.doi.org/10.1016/j.jngse.2016.07.012

Cui, X.J., Bustin, R.M., 2009. Measurements of gas permeability and diffusivity of tight reservoir rocks: different approaches and their applications. Geofluids 9 (3), 208–223.
Cui, X.J., Bustin, R.M., 2005. Volumetric strain associated with methane desorption and its impact on coalbed gas production from deep coal seams. AAPG Bull. 89, 1181–1202.
Curtis, M.E., Cardott, B.J., Songdergeld, C.H., Raia, C.S., 2012. Development of organic porosity in the Woodford shale with increasing thermal maturity. Int. J. Coal Geol. 103, 26–31.
Etminan, S.R., Javadpour, F, Maini, B.B., Chen, Z., 2014. Measurement of gas storage processes in shale and of the molecular diffusion coefficient in kerogen. Int. J. Coal Geol. 123, 10–19.
Florence, F.A., Rushing, J.A., Newsham, K.E., Blasingame, T.A., 2007. Improved permeability prediction relations for low-permeability sands. In: SPE Rocky Mountain Oil & Gas Technology Symposium. Denver, Colorado, USA, 18; SPE-107954.
Harpalani, S., Schraufnagel, R., 1990. Shrinkage of coal matrix with release of gas and its impact on permeability of coal. Fuel 69, 551–556.
Javadpour, F., Fisher, D., Unsworth, M., 2007. Nanoscale gas flow in shale gas sediments. J. Can. Pet. Tech. 46, 55–61.
Javadpour, F., 2009. Nanopores and apparent permeability of gas flow in mudrocks (shales and siltstone). J. Can. Pet. Tech. 48, 16–21.
Jin, G., Pfferez, H.G., Agrawal, G., Khodja, M.R., Ali, A.Z., Hussaini, S.R., Jangda, Z.Z., 2015. The impact of gas adsorption and composition on unconventional shale permeability measurement. In: SPE Middle East Oil & Gas Show and Conference. Society of Petroleum Engineers. SPE-172744.
Letham, E.A., 2011. Matrix Permeability Measurements of Gas Shales: Gas Slippage and Adsorption as Sources of Systematic Errors. BSc thesis. University of British Columbia, Vancouver, Canada.
Liu, J., Chen, Z., Elsworth, D., Qu, H., Chen, D., 2011a. Interactions of multiple processes during CBM extraction: a critical review. Int. J. Coal Geol. 87 (3–4), 175–189.
Liu, J., Chen, Z., Elsworth, D., Miao, X., Mao, X., 2011b. Evolution of coal permeability from stress-controlled to displacement-controlled swelling conditions. Fuel 90 (10), 2987–2997.
Liu, X.J., Xiong, J., Liang, L.X., 2015. Investigation of pore structure and fractal characteristics of organic-rich Yanchang formation shale in central China by nitrogen adsorption/desorption analysis. J. Nat. Gas Sci. Eng. 22, 62–72.
Neuzil, C., 1994. How permeable are clays and shales? Water Resour. Res. 30, 145–150.
Niu, C., Hao, Y.Z., Li, D.L., Lu, D.T., 2013. Second-order gas-permeability correlation of shale during slip flow. SPE J. 1–7.
Pan, Z., Connell, L.D., Camilleri, M., 2010. Laboratory characterisation of coal reservoir permeability for primary and enhanced coalbed methane recovery. Int. J. Coal Geol. 82, 252–261.
Pan, Z., Connell, L.D., 2011. Modelling of anisotropic coal swelling and its impact on permeability behaviour for primary and enhanced coalbed methane recovery. Int. J. Coal Geol. 85 (3–4), 257–267.
Rahmanian, M.R., Solano, N., Aguilera, R., 2010. Storage and output flow from shale and tight gas reservoirs. In: SPE Western Regional Meeting. Anaheim, California, USA, 21, SPE-133611.
Robertson, E.P., Christiansen, R.L., 2005. Measurement of sorption induced strain. In: Proceedings of the 2005 International Coalbed Methane Symposium. Tuscaloosa, AL, Paper 0532.
Sakhaee-Pour, A., Bryant, S., 2012. Gas permeability of shale. SPE Reserv. Eval. Eng. 103 (4), 401–409.
Sakurovs, R., Day, S., Weir, S., et al., 2007. Application of a modified Dubinin-Radushkevich equation to adsorption of gases by coals under supercritical conditions. Energy Fuels 21, 992–997.
Sakurovs, R., Day, S., Weir, S., Duffy, G., 2008. Temperature dependence of sorption of gases by coals and charcoals. Int. J. Coal Geol. 73 (3–4), 250–258.
Sakurovs, R., Day, S., Weir, S., 2009. Causes and consequences of errors in determining sorption capacity of coals for carbon dioxide at high pressure. Int. J. Coal Geol. 77, 16–22.
Sakurovs, R., Day, S., Weir, S., 2010. Relationships between the critical properties of gases and their high pressure sorption behavior on coals. Energy Fuels 24, 1781–1787.
Schloemer, S., Krooss, B.M., 1997. Experimental characterization of the hydrocarbon sealing efficiency of cap rocks. Mar. Pet. Geol. 14, 565–580.
Sigal, R.F., Akkutlu, I.Y., Kang, S.M., Diaz-Campos, M., Ambrose, R., 2013. The laboratory measurement of the gas storage capacity organic shales. Petrophysics 54, 224–235.
Sinha, S., Braun, E.M., Passey, Q.R., Leonardi, S.A., Boros, J.A., Wood III, A.C., Zirkle, T., Kudva, R.A., 2013. Steady-state permeability measurements on intact shale samples at reservoir conditions - effect of stress, temperature, pressure, and type of gas. In: SPE Middle East Oil and Gas Show and Conference. Manama, Bahrain SPE 164263:15–20.
White, C.M., Smith, D.H., Jones, K.L., Goodman, A.L., Jikich, S.A., LaCount, R.B., DuBose, S.B., Ozdemir, E., Morsi, B.I., Schroeder, K.T., 2005. Sequestration of carbon dioxide in coal with enhanced coal bed methane recovery - a review. Energy Fuels 19, 659–724.
Xiong, X., Devegowda, D., Michel, G.G., Sigal, R.F., Civan, F., 2012. A fully coupled free and adsorptive phase transport model for shale gas reservoirs including non-darcy flow effects. In: SPE Annual Technical Conference and Exhibition. San Antonio, Texas, USA SPE-159758.
Yu, W., Sepehrnoori, K., Patzek, T.W., 2014. Evaluation of gas adsorption in marcellus shale. In: SPE Annual Technical Conference and Exhibition. Amsterdam, The Netherlands 16:170801.

Please cite this article in press as: Wei, M., et al., Evolution of shale apparent permeability from stress-controlled to displacement-controlled conditions, Journal of Natural Gas Science and Engineering (2016), http://dx.doi.org/10.1016/j.jngse.2016.07.012